JOC*Article*

Nucleophilic Substitution at Silicon (S_N2@Si) via a Central Reaction Barrier

A. Patrícia Bento and F. Matthias Bickelhaupt*

Afdeling Theoretische Chemie, Scheikundig Laboratorium der Vrije Universiteit, De Boelelaan 1083, NL-1081 HV Amsterdam, The Netherlands

fm.bickelhaupt@few.vu.nl

Received January 12, 2007

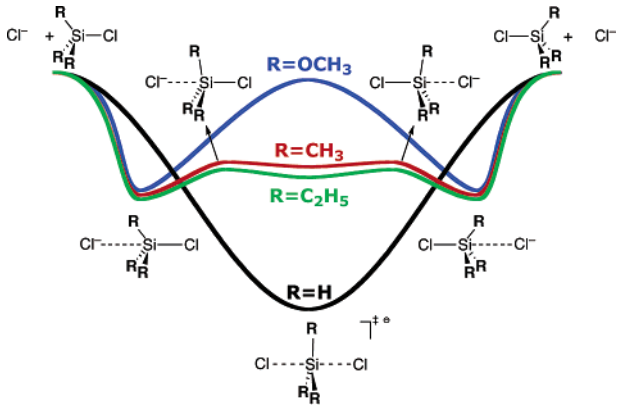

It is textbook knowledge that nucleophilic substitution at carbon (S_N2@C) proceeds via a central reaction barrier which disappears in the corresponding nucleophilic substitution reaction at silicon (S_N2@Si). Here, we address the question *why* the central barrier disappears from S_N2@C to S_N2@Si despite the fact that these processes are isostructural and isoelectronic. To this end, we have explored and analyzed the potential energy surfaces (PES) of various $Cl^- + CR_3Cl$ (R = H, CH_3) and $Cl^- + SiR_3Cl$ model reactions (R = H, CH_3, C_2H_5, and OCH_3). Our results show that the nature of the S_N2 reaction barrier is in essence steric, but that it can be modulated by electronic factors. Thus, simply by increasing the steric demand of the substituents R around the silicon atom, the S_N2@Si mechanism changes from its regular single-well PES (with a stable intermediate transition *complex*, TC), via a triple-well PES (with a pre- and a post-TS before and after the central TC), to a double-well PES (with a TS; R = OCH_3), which is normally encountered for S_N2@C reactions.

1. Introduction

Bimolecular nucleophilic substitution (S_N2) occurs in many synthetic organic approaches,[1] and various experimental and theoretical studies have been conducted to explore the potential energy surface (PES) and to understand the nature of this process.[2] The symmetric, thermoneutral S_N2 reaction between the chloride anion and chloromethane, $Cl^- + CH_3Cl$, in the gas phase is generally employed as the archetypal model for nucleophilic substitution. This reaction proceeds preferentially through a backside nucleophilic attack of the chloride anion at the carbon atom (S_N2@C) which goes with concerted expulsion of the leaving group. A well-known feature of gas-phase S_N2@C reactions is their double-well potential energy surface (PES) along the reaction coordinate which is characterized by a central barrier, provided by a trigonal bipyramidal transition state (TS), that separates two pronounced minima, associated with the reactant and product ion−molecule complexes (RC and PC).

* To whom correspondence should be addressed. Fax: +31-20-59 87629.

(1) March, J. *Advanced Organic Chemistry*, 4th ed.; Wiley-Interscience: New York, 1992.

(2) (a) Vayner, G.; Houk, K. N.; Jorgensen, W. L.; Brauman, J. I. *J. Am. Chem. Soc.* **2004**, *126*, 9054. (b) Gronert, S. *Acc. Chem. Res.* **2003**, *36*, 848. (c) Laerdahl, J. K.; Uggerud, E. *Int. J. Mass Spectrom.* **2002**, *214*, 277. (d) Chabinyc, M. L.; Craig, S. L.; Regan, C. K.; Brauman, J. I. *Science* **1998**, *279*, 1882. (e) Deng, L.; Branchadell, V.; Ziegler, T. *J. Am. Chem. Soc.* **1994**, *116*, 10645. (f) Shaik, S. S.; Schlegel, H. B.; Wolfe, S. *Theoretical Aspects of Physical Organic Chemistry: The S_N2 Reaction*; Wiley: New York, 1992. (g) Olmstead, W. N.; Brauman, J. I. *J. Am. Chem. Soc.* **1977**, *99*, 4219. (h) Glukhovtsev, M. N.; Pross, A.; Radom, L. *J. Am. Chem. Soc.* **1995**, *117*, 2024. (i) Botschwina, P. *Theor. Chem. Acc.* **1998**, *99*, 426. (j) Harder, S.; Streitwieser, A.; Petty, J. T.; Schleyer, P. v. *R. J. Am. Chem. Soc.* **1995**, *117*, 3253. (k) Chandrasekhar, J.; Smith, S. F.; Jorgensen, W. L. *J. Am. Chem. Soc.* **1985**, *107*, 154. (l) Lee, I.; Kim, C. K.; Sohn, C. K.; Li, H. G.; Lee, H. W. *J. Phys. Chem. A* **2002**, *106*, 1081. (m) Bickelhaupt, F. M. *J. Comput. Chem.* **1999**, *20*, 114. (n) Nibbering, N. M. M. *Acc. Chem. Res.* **1990**, *23*, 279. (o) DePuy, C. H.; Gronert, S.; Mullin, A.; Bierbaum, V. M. *J. Am. Chem. Soc.* **1990**, *112*, 8650.

10.1021/jo070076e CCC: $37.00
Published on Web 02/15/2007

The central reaction barrier disappears if we go to nucleophilic substitution at silicon (S_N2@Si)[3,4] or other third-period atoms.[5] This is often illustrated with the reactions of $Cl^- + CH_3Cl$ and $Cl^- + SiH_3Cl$: going from the former to the latter, the reaction profile changes from a double-well PES, involving a central TS, for substitution at a second-period atom (S_N2@C) to a single-well PES associated with a stable trigonal bipyramidal transition *complex* (TC) for substitution at the third-period congener (S_N2@Si). In certain instances, the formation of the stable trigonal bipyramidal TC has been found in early ab initio computations to proceed via a pre-transition state (pre-TS), for example, in the reactions of $RO^- + SiH_3CH_3$ with R = H and CH_3.[4c] However, these reaction barriers are not associated with the nucleophilic approach of RO^- toward Si. They rather originate from the energy-demanding return of a proton to the carbanion in the encounter complex [ROH···$^-CH_2SiH_3$] which is formed, at first, after spontaneous proton transfer from the methyl substituent in the substrate to the nucleophile.[4c]

Thus, nucleophilic substitution at carbon (S_N2@C) proceeds via a central reaction barrier which disappears in the corresponding nucleophilic substitution reaction at silicon (S_N2@Si). While this phenomenon as such is well-known, it is still not fully understood. The above S_N2@C and S_N2@Si substitutions are structurally equivalent and isoelectronic. *Why*, then, does the central reaction barrier disappear if we go from S_N2@C to the corresponding S_N2@Si process? And what causes the existence of a central barrier for S_N2@C in the first place? Is there an electronic factor responsible for the barrier in the case of S_N2@C (e.g., less favorable bonding capability of carbon compared to silicon), or is this barrier, as hypothesized by Dewar and Healy,[4b] steric in origin, that is, caused by repulsion between substituents around the smaller carbon atom?

To answer these questions, we have systematically analyzed and compared a series of archetypal S_N2@C and S_N2@Si reactions using the ADF program at OLYP/TZ2P.[6] This level of theory was previously shown to agree within a few kcal/mol with highly correlated ab initio benchmarks.[4a] Our model systems cover nucleophilic substitutions at carbon in CR_3Cl (eqs 1) and silicon in SiR_3Cl (eqs 2) with various substituents R = H, CH_3, C_2H_5, and OCH_3 that range from small to sterically more demanding. For comparison, we include into our discussion the nucleophilic substitutions at phosphorus (S_N2@P) shown in eqs 3, previously studied by van Bochove et al.[5a]

$$Cl^- + CH_3Cl \rightarrow CH_3Cl + Cl^- \quad (1a)$$

$$Cl^- + C(CH_3)_3Cl \rightarrow C(CH_3)_3Cl + Cl^- \quad (1b)$$

$$Cl^- + SiH_3Cl \rightarrow SiH_3Cl + Cl^- \quad (2a)$$

$$Cl^- + Si(CH_3)_3Cl \rightarrow Si(CH_3)_3Cl + Cl^- \quad (2b)$$

$$Cl^- + Si(C_2H_5)_3Cl \rightarrow Si(C_2H_5)_3Cl + Cl^- \quad (2c)$$

$$Cl^- + Si(OCH_3)_3Cl \rightarrow Si(OCH_3)_3Cl + Cl^- \quad (2d)$$

$$Cl^- + PH_2Cl \rightarrow PH_2Cl + Cl^- \quad (3a)$$

$$Cl^- + P(CH_3)_2Cl \rightarrow P(CH_3)_2Cl + Cl^- \quad (3b)$$

$$Cl^- + POH_2Cl \rightarrow POH_2Cl + Cl^- \quad (3c)$$

$$Cl^- + PO(CH_3)_2Cl \rightarrow PO(CH_3)_2Cl + Cl^- \quad (3d)$$

$$Cl^- + PO(OCH_3)_2Cl \rightarrow PO(OCH_3)_2Cl + Cl^- \quad (3e)$$

Our analyses reveal that steric congestion around carbon is indeed the origin of the barrier of S_N2@C reactions and that reduced steric repulsion around the larger silicon atom of a corresponding S_N2@Si reaction is the main reason for the disappearance of this central S_N2 barrier. Prompted by this finding, we have attempted to let the central reaction barrier reappear in the S_N2@Si reaction. Here, we anticipate that this attempt has been successful. We show how simply increasing the steric congestion at silicon shifts the S_N2@Si mechanism stepwise back from a single-well potential (with a stable central TC) that is common for substitution at third-period atoms, via a triple-well potential (featuring a pre- and post-TS before and after the central TC), back to the double-well potential (with a central TS!) that is well-known for substitution at carbon but unprecedented for substitution at silicon.

2. Theoretical Methods

Computational Details. All calculations were carried out with the Amsterdam Density Functional (ADF) program developed by Baerends and others.[6] The molecular orbitals (MOs) were expanded in a large uncontracted set of Slater-type orbitals (STOs) containing diffuse functions, TZ2P. The TZ2P basis set is of triple-ζ quality and has been augmented with two sets of polarization functions: 2p and 3d on hydrogen, and 3d and 4f on carbon, silicon, chlorine, and oxygen. The core shells of carbon (1s), silicon (1s2s2p), chlorine (1s2s2p), and oxygen (1s) were treated by the frozen-core

(3) (a) Elschenbroich, C. *Organometallics*; Wiley-VCH: Weinheim, Germany, 2006. (b) Sommer, L. H. *Stereochemistry, Mechanism, and Silicon*; McGraw-Hill: New York, 1965. (c) Holmes, R. R. *Chem. Rev.* **1990**, *90*, 17. (d) Damrauer, R.; Hankin, J. A. *Chem. Rev.* **1995**, *95*, 1137.

(4) (a) Bento, A. P.; Solà, M.; Bickelhaupt, F. M. *J. Comput. Chem.* **2005**, *26*, 1497. (b) Dewar, M. J. S.; Healy, E. *Organometallics* **1982**, *1*, 1705. (c) Sheldon, J. C.; Hayes, R. N.; Bowie, J. H. *J. Am. Chem. Soc.* **1984**, *106*, 7711. (d) Damrauer, R.; Burggraf, L. W.; Davis, L. P.; Gordon, M. S. *J. Am. Chem. Soc.* **1988**, *110*, 6601. (e) Windus, T. L.; Gordon, M. S.; Davis, L. P.; Burggraf, L. W. *J. Am. Chem. Soc.* **1994**, *116*, 3568. (f) Gronert, S.; Glaser, R.; Streitwieser, A. *J. Am. Chem. Soc.* **1989**, *111*, 3111. (g) DePuy, C. H.; Bierbaum, V. M.; Flippin, L. A.; Grabowski, J. J.; King, G. K.; Schmitt, R. J.; Sullivan, S. A. *J. Am. Chem. Soc.* **1980**, *102*, 5012. (h) Méndez, F.; Romero, M. L.; Gazquez, J. L. *J. Chem. Sci.* **2005**, *117*, 525. (i) Hilderbrandt, R. L.; Hommer, G. D.; Boudjouk, P. *J. Am. Chem. Soc.* **1976**, *98*, 7476. (j) Hao, C.; Kaspar, J. D.; Check, C. E.; Lobring, K. C.; Gilbert, T. M.; Sunderlin, L. S. *J. Phys. Chem. A* **2005**, *109*, 2026. (k) Shi, Z.; Boyd, R. J. *J. Phys. Chem.* **1991**, *95*, 4698. (l) Bowie, J. H. *Acc. Chem. Res.* **1980**, *13*, 76. (m) van der Wel, H.; Nibbering, N. M. M.; Sheldon, J. C.; Hayes, R. N.; Bowie, J. H. *J. Am. Chem. Soc.* **1987**, *109*, 5823. (n) Couzijn, E. P. A.; Ehlers, A. W.; Schakel, M.; Lammertsma, K. *J. Am. Chem. Soc.* **2006**, *128*, 13634.

(5) (a) van Bochove, M. A.; Swart, M.; Bickelhaupt, F. M. *J. Am. Chem. Soc.* **2006**, *128*, 10738. (b) Fish, C.; Green, M.; Kilby, R. J.; Lynam, J. M.; McGrady, J. E.; Pantazis, D. A.; Russell, C. A.; Whitwood, A. C.; Willans, C. E. *Angew. Chem.* **2006**, *118*, 3710; *Angew. Chem., Int. Ed.* **2006**, *45*, 3628. (c) Lahiri, S. D.; Zhang, G.; Dunaway-Mariano, D.; Allen, K. N. *Science* **2003**, *299*, 2067. (d) Sølling, T. I.; Pross, A.; Radom, L. *Int. J. Mass Spectrom.* **2001**, *210*, 1. (e) Bachrach, S. M.; Mulhearn, D. C. *J. Phys. Chem.* **1996**, *100*, 3535. (f) Bachrach, S. M.; Gailbreath, B. D. *J. Org. Chem.* **2001**, *66*, 2005. (g) Mulhearn, D. C.; Bachrach, S. M. *J. Am. Chem. Soc.* **1996**, *118*, 9415.

(6) (a) *ADF*, version 2005.01; Scientific Computing & Modelling (SCM): Amsterdam, The Netherlands. (b) te Velde, G.; Bickelhaupt, F. M.; Baerends, E. J.; Fonseca Guerra, C.; van Gisbergen, S. J. A.; Snijders, J. G.; Ziegler, T. *J. Comput. Chem.* **2001**, *22*, 931. (c) Fonseca Guerra, C.; Snijders, J. G.; te Velde, G.; Baerends, E. J. *Theor. Chem. Acc.* **1998**, *99*, 391.

approximation.[6b,7] An auxiliary set of s, p, d, f, and g STOs was used to fit the molecular density and to represent the Coulomb and exchange potentials accurately in each SCF cycle.

Energies and geometries were computed with the OLYP[8] density functional which involves Handy's optimized exchange, OPTX. Previous studies have shown that OLYP reaction profiles agree satisfactorily with highly correlated ab initio benchmarks.[4a,9,10] All stationary points were confirmed to be equilibrium structures (no imaginary frequencies) or a transition state[11] (one imaginary frequency) through vibrational analysis.[12] Furthermore, transition states were verified to connect the supposed educt and product minima by carrying out intrinsic reaction coordinate (IRC) calculations.[13]

Analysis of the Potential Energy Surfaces. Insight into how the activation barriers arise is obtained through Activation Strain analyses of the various model reactions.[14] The Activation Strain model[14] is a fragment approach to understanding chemical reactions in which the height of reaction barriers is described and understood in terms of the original reactants. Thus, the potential energy surface $\Delta E(\zeta)$ is decomposed, along the reaction coordinate ζ, into the strain $\Delta E_{strain}(\zeta)$ associated with deforming the individual reactants plus the actual interaction $\Delta E_{int}(\zeta)$ between the deformed reactants (eq 4).

$$\Delta E(\zeta) = \Delta E_{strain}(\zeta) + \Delta E_{int}(\zeta) \quad (4)$$

The strain $\Delta E_{strain}(\zeta)$ is determined by the rigidity of the reactants and on the extent to which groups must reorganize in a particular reaction mechanism, whereas the interaction $\Delta E_{int}(\zeta)$ between the reactants depends on their electronic structure and on how they are mutually oriented as they approach each other. It is the interplay between $\Delta E_{strain}(\zeta)$ and $\Delta E_{int}(\zeta)$ that determines if and at which point along ζ a barrier arises. The activation energy of a reaction $\Delta E^{\ddagger} = \Delta E(\zeta^{TS})$ consists of the activation strain $\Delta E^{\ddagger}_{strain} = \Delta E_{strain}(\zeta^{TS})$ plus the TS interaction $\Delta E^{\ddagger}_{int} = \Delta E_{int}(\zeta^{TS})$:

$$\Delta E^{\ddagger} = \Delta E^{\ddagger}_{strain} + \Delta E^{\ddagger}_{int} \quad (5)$$

The interaction $\Delta E_{int}(\zeta)$ between the strained reactants is further analyzed in the conceptual framework provided by the Kohn−Sham molecular orbital (KS−MO) model.[15] To this end, it is further decomposed into three physically meaningful terms:

$$\Delta E_{int}(\zeta) = \Delta V_{elstat} + \Delta E_{Pauli} + \Delta E_{oi} \quad (6)$$

The term ΔV_{elstat} corresponds to the classical electrostatic interaction between the unperturbed charge distributions of the deformed reactants and is usually attractive. The Pauli repulsion ΔE_{Pauli} comprises the destabilizing interactions between occupied orbitals and is responsible for any steric repulsion (see ref 15a for an exhaustive discussion). The orbital interaction ΔE_{oi} accounts for charge transfer (interaction between occupied orbitals on one moiety with unoccupied orbitals of the other, including the HOMO−LUMO interactions) and polarization (empty−occupied orbital mixing on one fragment due to the presence of another fragment). Since the Kohn−Sham MO method of density functional theory (DFT) in principle yields exact energies and, in practice, with the available density functionals for exchange and correlation, rather accurate energies, we have the special situation that a seemingly one-particle model (an MO method) in principle completely accounts for the bonding energy.[15a,b]

TABLE 1. Energies (in kcal/mol) Relative to Reactants of Stationary Points Occurring in S_N2@C, S_N2@Si, and S_N2@P Reactions[a]

no.	reaction	shape of PES[b]	RC	pre-TS	TS/TC
1a	$Cl^- + CH_3Cl$	double-well	−9.0	−	−0.1
1b	$Cl^- + C(CH_3)_3Cl$	double-well	−11.6	−	14.4
2a	$Cl^- + SiH_3Cl$	single-well	−	−	−24.4
2b	$Cl^- + Si(CH_3)_3Cl$	triple-well	−12.3	−9.1	−9.5
2c	$Cl^- + Si(C_2H_5)_3Cl$	triple-well	−12.8	−10.0	−10.7
2d	$Cl^- + Si(OCH_3)_3Cl$	double-well	−12.0	−	−1.2
3a[c]	$Cl^- + PH_2Cl$	single-well	−	−	−26.2
3b[c]	$Cl^- + P(CH_3)_2Cl$	triple-well	−13.0	−12.7	−15.6
3c[c]	$Cl^- + POH_2Cl$	single-well	−	−	−22.3
3d[c]	$Cl^- + PO(CH_3)_2Cl$	double-well	−16.2	−	−5.7
3e[c]	$Cl^- + PO(OCH_3)_2Cl$	double-well	−14.1	−	2.5

[a] Computed at OLYP/TZ2P; see Figure 1 for selected structures. [b] Shape of potential energy surface: either single-well (no TS), triple-well (two TSs), or double-well (one central TS). [c] From ref 5a.

3. Results and Discussion

Potential Energy Surfaces. The results of our OLYP/TZ2P computations are collected in Table 1 (energies) and Figure 1 (geometries). In the case of R = H, we recover the well-known change from a double-well PES with a central barrier and TS for S_N2@C (eq 1a) to a single-well PES for S_N2@Si (eq 2a) in which the pentavalent transition species has turned from a TS into a stable TC. The reactant complex (RC) of the S_N2@C reaction is bound by −9.0 kcal/mol, and it is separated from the product complex (PC) by a central barrier of +8.9 kcal/mol. The S_N2@Si reaction features only a stable pentacoordinate TC (no TS, RC, PC) at −24.4 kcal/mol. Previously, van Bochove et al.[5a] have shown that the PES of the S_N2@P reaction can be turned back from single-well (with a stable transition complex, TC) to double-well (with central transition state, TS) by increasing the steric demand of the substituents (see, for example, eqs 3 and the PES data in Table 1). This suggests that also S_N2@Si reactions may proceed via a double-well PES provided that substituents at silicon are sufficiently bulky.

Thus, we have probed the effect of replacing hydrogen by methyl or larger substituents R in the S_N2@Si (eqs 2) and, for comparison, the S_N2@C reactions (eqs 1). In the case of the latter, increasing the steric congestion at carbon causes an enormous increase of the central barrier: going from hydrogen (eq 1a) to methyl substituents (eq 1b) pushes the central barrier up from 8.9 to 26.0 kcal/mol (see Table 1). The PES of the more bulky S_N2@C reaction (eq 1b) remains double-well, with pronounced minima for RC and PC which are even slightly more stable (−11.6 kcal/mol) than those of the simple $Cl^- + CH_3Cl$ reaction (−9.0 kcal/mol; see Table 1 and Figure 1).

In the case of the corresponding S_N2@Si reactions, the introduction of the more bulky methyl substituents from reaction 2a to 2b causes the occurrence of a new feature on the PES,

(7) Baerends, E. J.; Ellis, D. E.; Ros, P. *Chem. Phys.* **1973**, *2*, 41.
(8) (a) Handy, N. C.; Cohen, A. J. *Mol. Phys.* **2001**, *99*, 403. (b) Lee, C.; Yang, W.; Parr, R. G. *Phys. Rev. B* **1988**, *37*, 785.
(9) (a) Swart, M.; Ehlers, A. W.; Lammertsma, K. *Mol. Phys.* **2004**, *102*, 2467. (b) Baker, J.; Pulay, P. *J. Chem. Phys.* **2002**, *117*, 1441. (c) Xu, X.; Goddard, W. A., III. *J. Phys. Chem. A* **2004**, *108*, 8495. (d) Gonzales, J. M.; Allen, W. D.; Schaefer, H. F., III. *J. Phys. Chem. A* **2005**, *109*, 10613.
(10) Gruning, M.; Gritsenko, O. V.; Baerends, E. J. *J. Phys. Chem. A* **2004**, *108*, 4459.
(11) Fan, L.; Ziegler, T. *J. Chem. Phys.* **1990**, *92*, 3645.
(12) Fan, L.; Versluis, L.; Ziegler, T.; Baerends, E. J.; Ravenek, W. *Int. J. Quantum Chem. Quantum Chem. Symp.* **1988**, *S22*, 173.
(13) Fukui, K. *Acc. Chem. Res.* **1981**, *14*, 363.
(14) (a) Diefenbach, A.; de Jong, G. Th.; Bickelhaupt, F. M. *J. Chem. Theory Comput.* **2005**, *1*, 286. (b) Diefenbach, A.; Bickelhaupt, F. M. *J. Chem. Phys.* **2001**, *115*, 4030. (c) Bickelhaupt, F. M. *J. Comput. Chem.* **1999**, *20*, 114.
(15) (a) Bickelhaupt, F. M.; Baerends, E. J. In *Reviews in Computational Chemistry*; Lipkowitz, K. B., Boyd, D. B., Eds.; Wiley-VCH: New York, 2000; Vol. 15, pp 1−86. (b) Baerends, E. J.; Gritsenko, O. V. *J. Phys. Chem. A* **1997**, *101*, 5383. (c) Ziegler, T.; Rauk, A. *Theor. Chim. Acta* **1977**, *46*, 1.

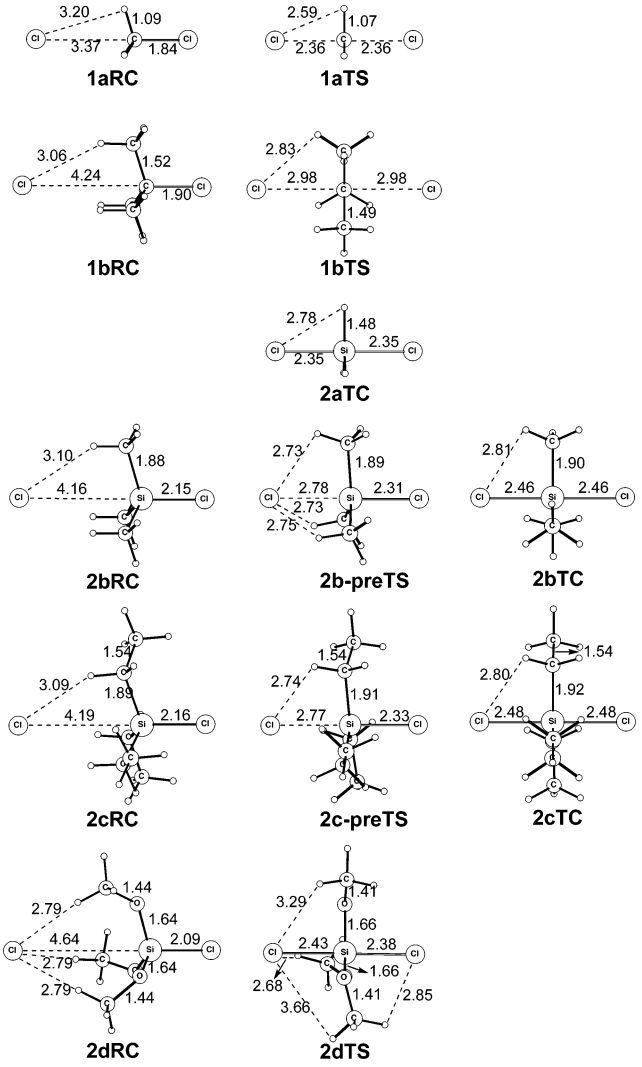

FIGURE 1. Structures (in Å; at OLYP/TZ2P) of selected stationary points for S_N2@C and S_N2@Si reactions.

namely, pre- and post-transition states that surround the central, pentavalent transition species **2bTC** (see Table 1 and Figure 1). The latter is again destabilized with respect to the transition complex **2aTC** in the corresponding reaction involving hydrogen substituents (eq 2a). However, **2bTC** is still a stable, intermediate complex; that is, it does not turn into a transition state. This finding is consistent with the results of Damrauer and coworkers[4d] who also found the $[ClSi(CH_3)_3Cl]^-$ species to be a stable siliconate intermediate. Note that, in this respect, the S_N2@Si reactions of $Cl^- + SiR_3Cl$ differ from the corresponding S_N2@P reactions of $Cl^- + POR_3Cl$ which show already a double-well PES with a central TS for R = CH_3 (see Table 1).[5a] Note, however, also that the pre- and post-barriers separating the stable **2bTC** from reactant and product complexes of reaction 2b are relatively small, only 0.4 kcal/mol (Table 1).

Interestingly, this suggests that further increasing the steric bulk of the substituents R in SiR_3Cl may eventually lead to a merging of the pre- and post-TS and a change from a triple-well to a double-well PES with a central, trigonal bipyramidal TS, also in the case of the S_N2@Si reactions. The change from triple- to double-well PES does not yet occur if we go from methyl (eq 2b) to ethyl substituents (eq 2c). Thus, in the reaction of $Cl^- + Si(C_2H_5)_3Cl$ (eq 2c), the RC, the pre-TS, as well as the TC are only slightly stabilized by 0.5, 0.9, and 1.2 kcal/mol, respectively (Table 1).

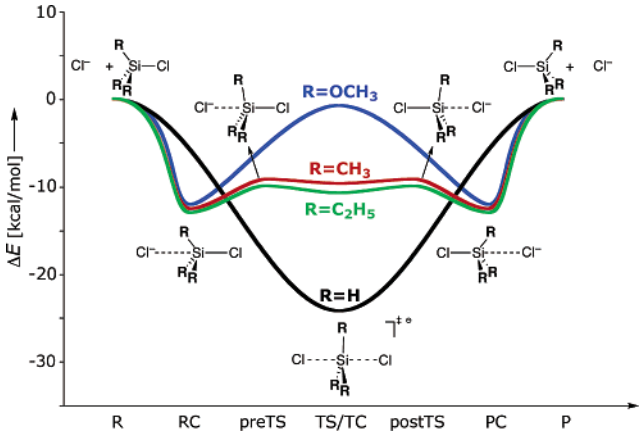

FIGURE 2. Potential energy surfaces ΔE along the reaction coordinate of the S_N2@Si reactions of $Cl^- + SiR_3Cl$ for R = H (black), CH_3 (red), C_2H_5 (green), and OCH_3 (blue), computed at OLYP/TZ2P.

The introduction of methoxy substituents (eq 2d) finally causes the pre- and post-TS to merge into one central TS that occurs at the trigonal bipyramidal transition structure **2dTS** (see Table 1 and Figure 1). Our analyses reveal that this originates from a further increase of steric repulsion around the congested pentacoordinate silicon (vide infra). Thus, we arrive at a RC and PC that are each bound by −12.0 kcal/mol and separated by a central barrier of +10.8 kcal/mol. In **2dTS**, one methoxy group is within the numerical precision symmetrically oriented between nucleophile and leaving group, whereas the other two methoxy groups point either slightly to the nucleophile or the leaving group, respectively (see Figure 1). A full IRC analysis without any symmetry restriction confirms that **2dTS** is indeed the first-order saddle point that connects **2dRC** and **2dPC** on the multidimensional PES.

To the best of our knowledge, this is the first example of an S_N2@Si reaction that proceeds via the classical double-well potential. Figure 2 illustrates how the increasing steric demand of the substituents R in the substrate SiR_3Cl, along R = H, CH_3, C_2H_5, and OCH_3 in reactions 2a−d, first causes the occurrence of steric pre- and post-barriers (R = CH_3 and C_2H_5) which eventually merge into one central barrier (R = OCH_3).

Activation Strain Analyses of the Model Reactions. Next, we address the steric nature of the various S_N2 reaction barriers that was already mentioned in the discussion above. The insight that these barriers are in most cases steric emerges from our Activation Strain analyses[14] in which the potential energy surface $\Delta E(\zeta)$ of the model reactions is decomposed, along the reaction coordinate ζ, into the strain $\Delta E_{strain}(\zeta)$ associated with deforming the individual reactants plus the actual interaction $\Delta E_{int}(\zeta)$ between the deformed reactants (eq 4; for details, see section 2). The results of the Activation Strain analyses are collected in Figure 3 in which we show the S_N2 potential energy surface $\Delta E(\zeta)$ (left panel), its decomposition into $\Delta E_{strain}(\zeta) + \Delta E_{int}(\zeta)$ (middle panel), and the decomposition of the nucleophile−substrate interactions $\Delta E_{int}(\zeta)$ (right panel) of $Cl^- + CH_3Cl$ (1a), SiH_3Cl (2a), $Si(CH_3)_3Cl$ (2b), $Si(C_2H_5)_3Cl$ (2c), and $Si(OCH_3)_3Cl$ (2d).

For each reaction, three situations are analyzed, which are distinguished in the illustrations by a color code: black, blue, and red curves. The black lines refer to the regular internal reaction coordinate (IRC). Here, the IRC is modeled by a linear

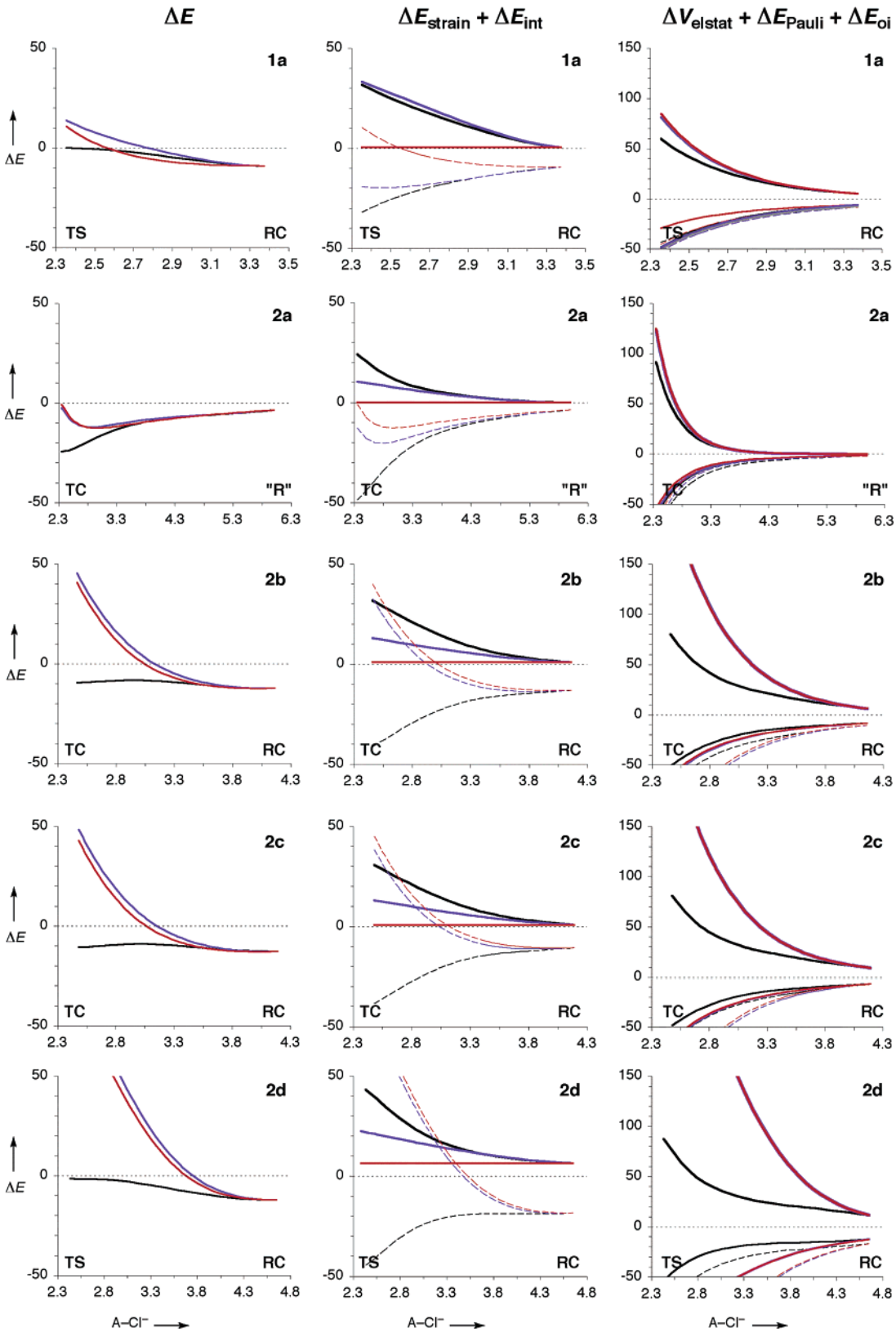

FIGURE 3. Analysis of the potential energy surfaces ΔE (in kcal/mol) of the S_N2 reactions of $Cl^- + CH_3Cl$ (eq 1a) and $Cl^- + SiR_3Cl$ for R = H (2a), CH_3 (2b), C_2H_5 (2c), and OCH_3 (2d) along the reaction coordinate projected onto the Cl^-−Si (or Cl^-−C) distance (in Å). Left panel: Potential energy surfaces ΔE. Middle panel: Activation Strain analysis of the potential energy surfaces $\Delta E = \Delta E_{strain}$ (bold lines) + ΔE_{int} (dashed lines). Right panel: Energy decomposition of the nucleophile−substrate interaction $\Delta E_{int} = \Delta V_{elstat}$ (dashed lines) + ΔE_{Pauli} (bold lines) + ΔE_{oi} (plain lines). Black lines: Regular internal reaction coordinate (IRC). Blue lines: IRC with geometry of $[CH_3]$ or $[SiR_3]$ unit in substrate frozen to that in the reactant complex (RC) or reactants ("R"). Red lines: IRC with geometry of entire substrate frozen to that in the RC or "R".

transit in which the nucleophile−central atom distance and the central atom−leaving group distance run synchronously from their value in the RC to that in the central transition structure, TS or TC, in 50 steps. All other geometrical degrees of freedom are fully optimized at each step. In those instances, in which no RC exists, the IRC runs from a geometry that closely resembles the separate reactants ("R") to the TC, where "R" is defined by a nucleophile−central atom distance of 6 Å and the central atom−leaving group distance in the equilibrium structure of the substrate. Next, the analyses represented in blue lines refer to the situation in which the geometry of the substrate is kept frozen to its geometry in the RC (or "R"), except for the central atom−leaving group distance and relative orientation; that is, the $[CH_3]$ or $[SiR_3]$ moiety is frozen, but the leaving group still departs as the nucleophile approaches. The red lines, finally, refer to analyses in which the entire substrate is frozen to the geometry it adopts in the RC or to its equilibrium geometry ("R").

Nucleophilic Substitution at Carbon. First, we analyze the S_N2@C of $Cl^- + CH_3Cl$ (eq 1a). As the reaction progresses from the RC to the TS, the energy ΔE rises from −9 to 0 kcal/mol (black line in Figure 3, left panel; see also Table 1). In terms of the Activation Strain model, this is so because the stabilization from the nucleophile−substrate interaction ΔE_{int} is not sufficiently stabilizing to compensate the strain ΔE_{strain} that is building up in the substrate (bold black line in Figure 3, middle panel).

The origin of this build up of strain turns out to be steric congestion around the carbon atom of the substrate. This congestion induces a structural deformation in the substrate that partially relieves the steric repulsion (see also ref 5a). The nucleophile−substituent (Cl^-−H) distance in **1aTS** is only 2.59 Å, significantly shorter than the 3.20 Å in **1aRC** (see Figure 1). This distance would be even shorter if the H substituents would not bend away yielding a planar CH_3 moiety in the TS. Indeed, if we freeze the $[CH_3]$ moiety in its pyramidal geometry of the RC, the energy ΔE goes up by 14 kcal/mol at the TS (compare blue and black curves in Figure 3, left 1a). This is nearly entirely due to a reduction by 12 kcal/mol in the nucleophile−substrate interaction ΔE_{int} (compare blue and black dashed lines in Figure 3, middle 1a). The reason that ΔE_{int} is substantially weakened appears to be a substantial rise in Pauli repulsion between the Cl^- 3p AOs and C−H bonding orbitals on CH_3Cl (see rise from black to blue bold lines in Figure 3, right 1a). The bonding orbital interactions ΔE_{oi} as well as the electrostatic attraction ΔV_{elstat} are hardly affected.

The build up of substrate strain can only be avoided by completely freezing the substrate to the geometry it adopts in the RC, in which case the carbon−leaving group distance remains fixed at the short value of 1.84 Å (see **1aRC** in Figure 1). One might expect the barrier on the PES to collapse as the strain at the TS drops by some 30 kcal/mol to practically[16] zero (see red bold line in Figure 3, middle 1a). However, this is not the case. The barrier goes down by only 3 kcal/mol compared to the partially frozen situation! This is because the nucleophile−substrate interaction ΔE_{int} (which is now approximately equal to ΔE) is enormously destabilized and even becomes repulsive near the TS (compare red and blue dashed lines in Figure 3, middle 1a). The reason is not a further increase of the Pauli repulsion which remains practically unchanged (red and blue bold lines nearly coincide in Figure 3, right 1a). This is what one would expect as the steric appearance of the substrate, that is, the frozen CH_3 moiety, is the same in both simulations. The destabilization in ΔE_{int} can be traced to a comparable loss in bonding orbital interactions ΔE_{oi} (compare red and blue plain lines in Figure 3, right 1a). The origin is that the donor−acceptor interaction between the Cl^- 3p AO and the CH_3Cl σ^*_{C-Cl} LUMO normally (black but also blue lines) induces an elongation in the carbon−leaving group bond which amplifies this stabilizing interaction because it leads to a lowering of the σ^*_{C-Cl} orbital and thus a smaller, that is, more favorable HOMO−LUMO gap. This effect has been switched off by not allowing the carbon−leaving group bond to expand. The orbital interactions still increase as the nucleophile approaches because the $<3p|\sigma^*_{C-Cl}>$ overlap increases, but they do so much less efficiently than when the carbon−leaving group bond is free to expand.

Nucleophilic Substitution at Silicon. The above results suggest that, by decreasing the steric congestion at the central atom and by strengthening the nucleophile−substrate interaction, one can let the S_N2 central barrier disappear, and this is exactly what happens if we go from $Cl^- + CH_3Cl$ (1a) to the S_N2@Si reaction of $Cl^- + SiH_3Cl$ (2a). The TS turns into a stable pentacoordinate TC (vide supra) because both the strain and interaction curves are significantly stabilized; at the transition structure, ΔE_{strain} decreases from 32 to 24 kcal/mol and ΔE_{int} goes from −32 to −49 kcal/mol (Figure 3, compare black bold lines in 1a and 2a middle).

Despite these obvious differences, the strain and interaction curves of the S_N2@Si reaction of $Cl^- + SiH_3Cl$ (2a) have still the same origin as in the case of the S_N2@C reaction of $Cl^- + CH_3Cl$ (1a). The strain still originates from steric repulsion between the approaching nucleophile and the substituents around the silicon atom which is partially relieved by structural deformation of the substrate. Thus, if we freeze the $[SiH_3]$ moiety in its pyramidal geometry in the reactants "R" (i.e., in free SiH_3Cl), the energy ΔE rises by 22 kcal/mol at the TC (Figure 3, compare blue and black curves in 2a left). This occurs despite a drop in strain that results from switching off the planarization of $[SiH_3]$ (Figure 3, compare black bold lines in 1a and 2a middle) and is exclusively caused by a weakening in the nucleophile−substrate interaction ΔE_{int} by 35 kcal/mol at the TC (Figure 3, compare blue and black dashed lines in 2a middle). The reason that ΔE_{int} is substantially weakened appears to be again the substantial rise in steric (Pauli) repulsion between the Cl^- 3p AOs and Si−H bonding orbitals on SiH_3Cl (Figure 3, see rise from black to blue bold lines in 1a right). The bonding orbital interactions ΔE_{oi} as well as the electrostatic attraction ΔV_{elstat} are much less affected by freezing the $[SiH_3]$ moiety.

Freezing the entire substrate SiH_3Cl in its equilibrium geometry does not have much effect on the PES ΔE. This behavior as well as its origin is again similar to that for the S_N2@C reaction 1a; on one hand, the strain ΔE_{strain} to collapse to zero but, at the same time, the nucleophile−substrate interaction ΔE_{int} is destabilized by a comparable amount (see Figure 3, compare red and blue lines in 2a middle). The origin of the weakening in ΔE_{int} is that the donor−acceptor interaction between the Cl^- 3p AO and the SiH_3Cl σ^*_{Si-Cl} LUMO normally (Figure 3, black and blue plain lines in 2a right) benefits from the elongation in the silicon−leaving group bond which

(16) (a) ΔE_{strain} is +0.4 kcal/mol and not exactly 0.0 kcal/mol because the $[CH_3Cl]$ moiety is kept frozen to its geometry in the RC, which is already slightly deformed with respect to the equilibrium geometry of isolated chloromethane because of the interaction with the chloride anion.

amplifies this stabilizing interaction because it leads to a lowering of the σ^*_{Si-Cl} orbital and thus a smaller, that is, more favorable HOMO−LUMO gap. This effect has been switched off by not allowing the silicon−leaving group bond to expand.

Introducing Bulky Substituents. Thus, from S_N2@C reaction 1a to S_N2@Si reaction 2a, the central barrier disappears because the steric congestion at the larger silicon atom is reduced and because the nucleophile−substrate interaction in the latter is more favorable. This suggests that, as observed above, S_N2@Si substitution of $Cl^- + SiR_3Cl$ may be turned into a process that proceeds via a double-well PES with a central barrier, similar to S_N2@C reactions, simply by sufficiently increasing the steric bulk of the substituents R.

The steric congestion at the central atom and, indeed, the similarity with the S_N2@C reaction (1a) increase along the S_N2@Si reactions of $Cl^- + SiH_3Cl$ (2a), $Si(CH_3)_3Cl$ (2b), and $Si(C_2H_5)_3Cl$ (2c). Introducing the more bulky methyl or ethyl substituents tremendously boosts the Pauli repulsion ΔE_{Pauli} in the fictitious process in which the $[SiR_3]$ moiety is kept frozen pyramidal in reactions 2b and 2c if compared to the corresponding process with a frozen $[SiH_3]$ unit in reaction 2a (Figure 3, compare blue bold lines in right 2b,c vs 2a). Note that the differences between reactions 2b and 2c are comparatively small. Apparently, methyl and ethyl substituents have a similar steric demand in the vicinity of the central atom to which our monatomic nucleophile approaches. Pauli repulsion is converted into substrate strain in the real S_N2@Si processes 2b and 2c, in which the substrate deformation is not suppressed (Figure 3, compare black and blue bold lines in middle and right 2b and 2c). Thus, from reaction 2a to reactions 2b and 2c, the strain at the TC increases strongly from 24 to some 32 kcal/mol. This destabilizing effect is further reinforced by a weakening in the nucleophile−substrate interaction ΔE_{int} from −49 kcal/mol for reaction 2a to ca. −40 kcal/mol for reactions 2b and 2c. The increased steric repulsion (converted into substrate strain) from reaction 2a to 2b and 2c causes the pre- and post-barriers mentioned above to lift off from the PES. The transition structure is also destabilized, from −24 to ca. −10 kcal/mol, but it still remains a stable TC (see Table 1). Thus, we arrive at a triple-well PES for reactions 2b and 2c featuring pre- and post-barriers that separate the stable pentavalent TC from reactant and product complexes.

In the case of S_N2@P substitution at tetracoordinate phosphorus, going from hydrogen (reaction 3c) to methyl substituents (reaction 3d) is already sufficient to let the pre- and post-barrier merge into one central barrier and, thus, to arrive at a double-well PES (see Table 1). This is consistent with the fact that the phosphorus atom is slightly smaller and therefore more sensitive to steric congestion than the silicon atom. For example, in the TC of $Cl^- + POH_2Cl$ (3c), the Pauli repulsion between the reactants is 104 kcal/mol, while in the TC of $Cl^- + SiH_3Cl$ (2a), this value is only 91 kcal/mol (compare Figure 3 with Figure 3 in ref 5a).

Finally, going from methyl or ethyl substituents R in $Cl^- + SiR_3Cl$ (2b, 2c) to methoxy substituents in $Cl^- + Si(CH_3O)_3Cl$ (2d), the steric bulk becomes sufficiently large to outweigh the favorable nucleophile−substrate interaction and to bring back the double-well potential with a central S_N2 barrier. The Pauli repulsion ΔE_{Pauli} in the fictitious process in which the $[SiR_3]$ moieties are kept frozen pyramidal jumps from 214 (2b) or 229 (2c) to 411 kcal/mol (2d) at the transition structure. In fact, the ΔE_{Pauli} curve of the latter S_N2@Si (2d) runs, already early, of the scale in the illustration; compare blue (behind red) bold lines in Figure 3, right 2d versus 2c. The increased Pauli repulsion translates again into a higher strain energy in the real, unconstrained S_N2@Si reaction 2d (Figure 3, middle 2d). The nucleophile−substrate interaction does not change that much from 2c to 2d. Thus, the increased steric bulk forces the central reaction barrier to reappear in this S_N2@Si substitution.

4. Conclusions

The central barrier in S_N2 reactions is determined by the interplay of steric and electronic effects, such as Pauli repulsion between the substituents (including nucleophile and leaving group) at the central atom and donor−acceptor orbital interactions between nucleophile and substrate. From S_N2@C in $Cl^- + CH_3Cl$ to S_N2@Si in $Cl^- + SiH_3Cl$, the central barrier disappears because there is less steric congestion and a more favorable interaction. However, the central barrier reappears as the steric bulk around the silicon atom is raised along the model reactions $Cl^- + SiH_3Cl$, $Si(CH_3)_3Cl$, and $Si(OCH_3)_3Cl$. To the best of our knowledge, this is the first example of an S_N2@Si reaction that proceeds via the classical double-well potential with a central reaction barrier. Our results highlight, once more,[5a] the steric nature of the S_N2 barrier in general.[17]

Acknowledgment. We thank The Netherlands Organization for Scientific Research (NWO-CW) for financial support.

Supporting Information Available: Cartesian coordinates of all species occurring in our model reactions. This material is available free of charge via the Internet at http://pubs.acs.org.

JO070076E

(17) For the role of steric repulsion in determining equilibrium geometries, see also: (a) Ref 15a. (b) Bickelhaupt, F. M.; DeKock, R. L.; Baerends, E. J. *J. Am. Chem. Soc.* **2002**, *124*, 1500. (c) Bickelhaupt, F. M.; Baerends, E. J. *Angew. Chem.* **2003**, *115*, 4315; *Angew. Chem., Int. Ed.* **2003**, *42*, 4183.